A Technique for the Quantitative Spatial Analysis of Sea Ice Melt Features Using Low Level Aerial Photographs

C.P. DERKSEN[1], J.M. PIWOWAR[1] AND E.F. LEDREW[1]

ABSTRACT

The transition from a dry snow cover over Arctic sea ice to a prevalence of melt pond features can occur quickly - on the order of two weeks or less. As the energy absorption and scattering properties of a ponded sea ice surface differ radically from those of a snow covered surface, calculating the rate at which the snow cover to melt pond ratio changes is of great significance. With a high spatial resolution, low level aerial photographs are an excellent data source for monitoring the evolution of sea ice melt features. This study outlines the analysis methods applied to a time series of aerial photographs in order to quantify the evolution of melt pond coverage through the spring melt season. Results indicate that an approximate maximum of 50% of the sea ice surface became covered by melt features. The growth rate of melt feature class through the time series of imagery was nearly linear. Discussion focusses on modelling applications, links to meteorological variables, and technical considerations.

Key words: sea ice, melt ponds, aerial photography

INTRODUCTION

Arctic sea ice and its overlying snow pack comprise both a spatially and temporally variable medium. From ice formation in the fall to relatively static conditions through the winter months to ice decay in the spring and summer, the sea ice surface changes greatly through time. Within the individual seasonal periods there exists great spatial variance in sea ice properties as well. For example, while melt features are forming on the ice surface in spring, patches of residual snow cover can exist long after a high proportion of surface flooding has been reached.

Remotely sensed imagery is an ideal data source for monitoring changes in sea ice surface parameters through time (i.e. Scharfen et al., 1987) and the fine spatial resolution of aerial photographs make them well suited for monitoring the spatial evolution of melt features. This study presents the methodology used to calculate the changing proportion of melt pond surface area to residual snow cover over first-year sea ice using imagery collected during the 1995 Seasonal Sea Ice Monitoring and Modelling Site (SIMMS) field experiment in the Canadian Arctic Archipelago. This work will focus on the necessary procedures to modify raw photographs into binary class images of melt feature and residual snow cover from which the changing proportion of those classes can be calculated over time. Results from an intensive study area will be presented along with data from spatially disparate images to investigate the consistency of results.

Implications of the changing surface properties of sea ice include differences in energy exchange at the ice/atmosphere interface, and a variable surface albedo which is intimately linked to the degree of surface ponding (Langleben, 1971). An accurate quantification of the changing spatial coverage of melt ponds, and corresponding surface albedo is important to the derivation of regional surface albedo as thermodynamic sea ice models have shown great sensitivity to that parameter (Shine and Henderson-Sellers, 1985). Sea ice modeling efforts may also be sensitive to other melt feature variables, such as pond depth, but these are not investigated here. (Ebert and Curry, 1993).

Melt Pond Formation

The processes of ice and snow ablation are complex and not well understood, however the relationship between ice decay and albedo can be illustrated well with the following positive feedback cycle. (For a more thorough discussion see Ingram et al., 1988.) The snow covered sea ice surface has a uniformly high surface albedo during winter and early spring. This reflection of nearly all incident radiation along with consistently cold surface temperatures maintains relatively static ice conditions. The spring transition is marked by increased ambient temperature, increased incident solar radiation, extensive cloud cover, and more precipitation. Snow pack temperature rises along with air temperature creating a markedly wetter snow volume. This increase in snow pack water content lowers the surface albedo so energy absorption increases. The snow pack warming process is further enhanced by this increase in energy absorption and melt features begin to form on the surface. The actual spatial distribution of melt

[1] Department of Geography, University of Waterloo, Waterloo, Ontario, Canada N2L 3G1

ponds is dependent on surface characteristics such as snow cover and ice roughness. Standing water within melt features act as solar radiation sinks, greatly increasing energy absorption and accelerating the further formation of deeper, more extensive ponds. The initial onset of melt can be slow to occur, however once water becomes present in the snow pack, the rapid development of melt pond features is triggered.

General spring Arctic sea ice conditions are marked by a melt which initiates in late May to early June, with the appearance of the first small and shallow melt ponds. Pond area increases to a maximum in mid-July although areas of melt water drainage occur through leads, cracks, and seal breathing holes.

DATA

Low level aerial photographs of a first-year sea ice study area were collected from a tethered balloon as a component of the SIMMS'95 field season conducted near Resolute NT (Fig. 1). SIMMS is a multi-disciplinary field experiment which operated from Day 94 (April 4) to Day 170 (June 19) 1995 with balloon flights occurring daily from Day 158 (June 7) to Day 170 (June 19). This analysis focuses on a time series of images collected at a balloon flying height of 300 meters with photographic infrared film. Panchromatic photographs were also collected simultaneously although they were not used in the present analysis because they are not as useful for discriminating melt features.

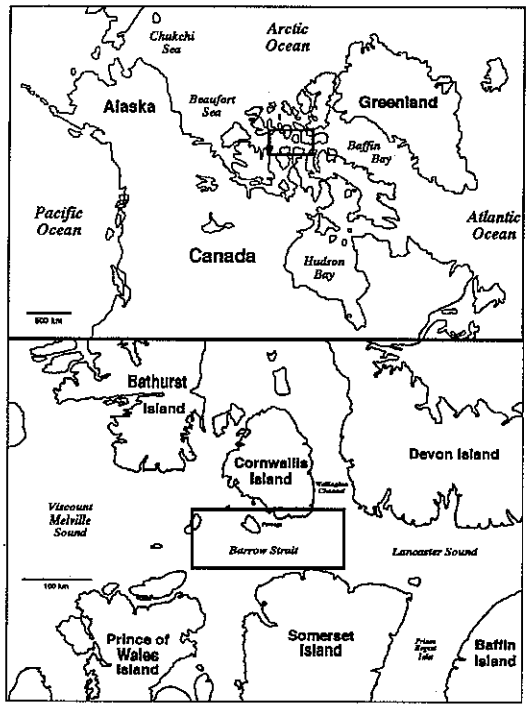

Figure 1. The SIMMS'95 study area.

Cameras were attached to a gimbal mount and suspended below a helium filled Raven Industries TRF-900 balloon (Figure 2). Complete technical details are given in Piwowar (1995). After the field season the photographs were scanned into digital images for analysis at a resolution of 1536 pixels by 1024 lines. Surface measurements were also collected in conjunction with the balloon photography. An Analytical Spectral Devices Personal Spectrometer II was used to measure surface radiance between 300 and 1000 nm at selected ponds each day. Pond depth, colour, and bottom texture were also noted. These surface measurements will be integrated into future research.

A three step image manipulation procedure was used to prepare the photography for the digital analysis of melt feature to snow cover ratios.

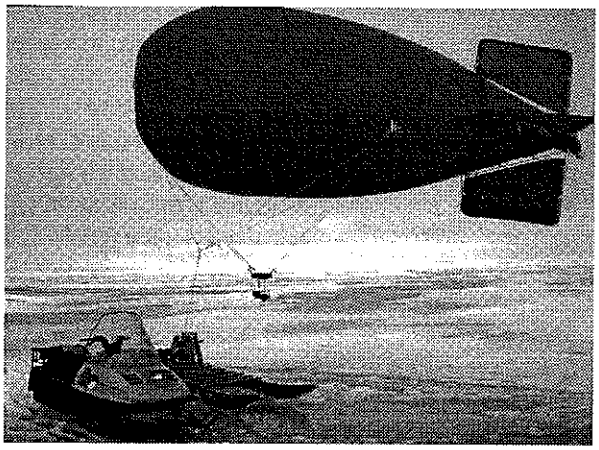

Figure 2. Balloon setup used for acquiring images.

1. Image Registration

Although the balloon was flown over the same study area each day, wind induced drift created changes in the photographic coverage of each image. In order to isolate a common area, the time series of data were co-registered using the PCI Image Analysis System (V 5.3). Black cloth markers laid down in the field were used as ground control points for the co-registration procedure and were very effective during the early spring season, although their utility diminished considerably as melt progressed and surface water eventually covered the markers. The RMS position error during the co-registration procedure was consistently below 1 pixel, and therefore considered acceptable. Certain days in the time series (Table 1) were omitted because of poor image quality due to foggy conditions which are prevalent during this season.

Table 1. Image acquisition days and times

Day	*Time*	*Day*	*Time*	*Day*	*Time*
158	1745	160	1200	167	1230
159	1200	160	1700	169	1200
159	1700	163	1300		

2. Image Enhancement/Noise Reduction

The next step of the analysis procedure involved the segmenation of the raw images into binary classes of melt feature and snow cover. This proved to be rather difficult for a number of reasons. During melt onset, young, shallow melt features and an increasingly wet snow pack have overlapping gray tones which are highly speckled and therefore cannot be thresholded into binary classes (Figure 3a). As the melt progresses, areas of standing water deeper than 10 cm become very clear as they return a consistent, dark gray tone on the infrared film, however transitional melt features which consist of shallow water or an extremely wet snow pack share similar gray tones to the residual snow cover (Figure 3b). This problem again leads to thresholding inaccuracies. Image modification techniques were therefore explored to enhance contrast between melt features and snow cover and to reduce image noise.

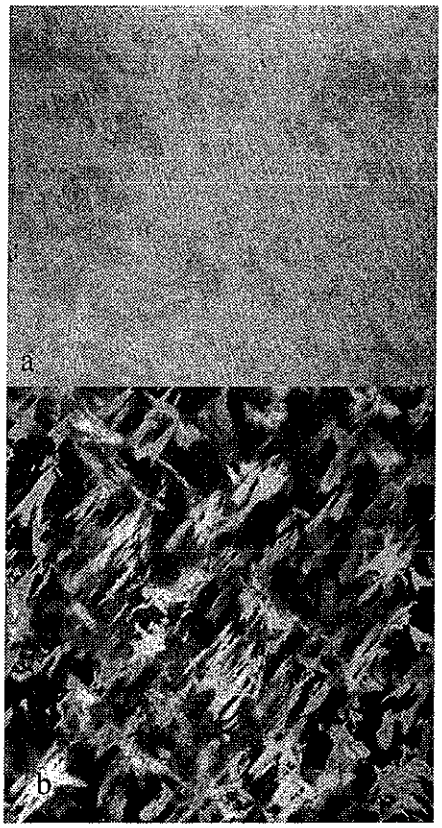

Figure 3. Raw aerial photographs from early melt (a) and late melt (b).

Numerous techniques were explored with a wide range of results. Simple neighbourhood texture operators such pixel range and pixel variance (Russ, 1995) failed to improve image segmentation significantly. A Hurst co-efficient (Russ, 1995) was calculated and applied to octagonal neighbourhoods and improved contrast between feature classes, however the results did not warrant pursuing this time consuming method. It was concluded that the greatest image noise reduction with acceptable time and computational committment was achieved using a median filter, with which the center pixel in a 3 x 3 neighbourhood was replaced by the median pixel value in that neighbourhood. This technique reduced image noise and speckle, improved contrast between melt features and snow cover, and the integrity of fine discontinuous zones between water and snow was maintained. For these reasons, the entire time series of images was processed with the median filter.

The noise reduction procedure was a vital step that ensured accurate image segmentation. The contour plots of pixel gray values shown in Figures 4 to 6 graphically show the changes and improvements attained with the use of the median filter. Raw and noise reduced images from Day 159 are shown in Figure 4. There is very little surface ponding at this time but the snowpack is getting continually wetter. Bare ice areas appear darker than snow covered areas, with the bare ice areas eventually becoming melt ponds (Derksen et al., 1996). As shown in Figure 4a it is not possible to differentiate any image classes due to image speckle. Image noise dominates any thresholding procedure. After image enhancement some noise is still present, however it is possible to more clearly differentiate between classes (Figure 4b).

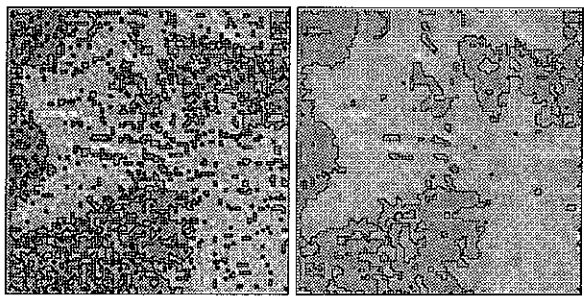

Figure 4. Raw (left) and median filtered (right) images from Day 159 with pixel value contours overlaid.

By Day 163 (Figure 5), melt is underway with some surface ponding occurring. Before the application of the noise reduction procedure, there can be some isolation of image classes (Figure 5a), but this is greatly improved after image enhancement (Figure 5b). Three clear classes emerge in Figure 5b: standing water (dark gray), transitional melt features or saturated snow cover (light gray), and residual snow cover (white).

Late melt season imagery from Day 169 is shown in Figure 6. Accurate image segmentation becomes easier by this time of year as melt ponds become deeper and are therefore more spectrally unique from any surrounding snow cover. Even without image enhancement, segmentation is acceptable (Figure 6a). The main benefit from image

segmentation, after noise reduction, is the improved classification of transitional melt features as highlighted in Figure 6b.

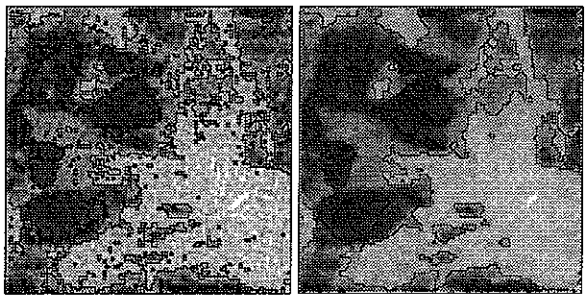

Figure 5. Raw (left) and median filtered (right) images from Day 163 with pixel value contours overlaid. Note the three clean image classes on the enhanced image: melt feature (dark gray), transitional melt feature (light gray), and snow cover (white).

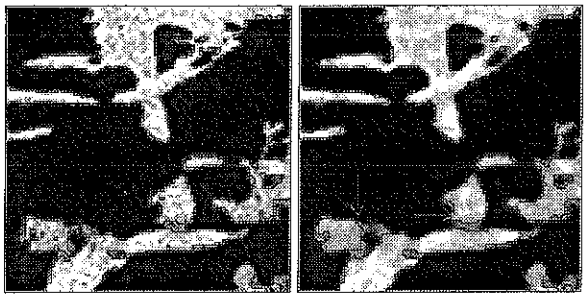

Figure 6. Raw (left) and median filtered (right) images from Day 169 with pixel value contours overlaid. Arrows point out some of the small transitional melt areas (light gray) that only become clear after median filtering.

3. Image Thresholding

The thresholding procedure converted the noise reduced data into a binary image comprised of melt feature and residual snow cover classes. From these images, the ratio of melt feature area to residual snow cover area can be calculated easily. A consistent gray level could not be used as the threshold value across the entire time series for two reasons. First, differences in lighting conditions which occurred between and within days, darkened or lightened the overall tone of the images. For example, images collected under diffusely lit conditions were comprised of darker gray tones than images collected under clear skies. Subsequently, diffusely lit images required a lower threshold value to accurately demarcate snow cover from melt features.

Secondly, melt features appear darker as depth increases so late season melt ponds are considerably darker than early season ponds. Additionally, increased snowpack wetness also results in darker gray levels meaning the threshold value had to be constantly adjusted to account for changes in the tone of transitional melt features and the wet snow cover. In summary, a unique threshold level was subjectively chosen for each image in response to the conditions discussed above.

RESULTS

The primary goal of this work was to establish the rate at which the ratio of snow cover to melt feature areal extent changes on first-year Arctic sea ice during the spring melt period. Calculations using low level aerial photographs show a strong linear growth rate from the onset of melt to approximately a 50:50 snow cover:melt feature ratio (Figure 7). The first day of imagery used in the analysis (Day 159) had no standing water or apparent melt features in the study area. During Day 160 melt feature growth started slowly and progressed to 8% spatial coverage in one day. By Day 163, 25% of the image area was in the melt feature class and this growth trend continued until Day 169 when just over 53% of the study area was classified as melt feature. At this point the growth trend appears to level off with no significant change in melt pond area occurring within Day 169.

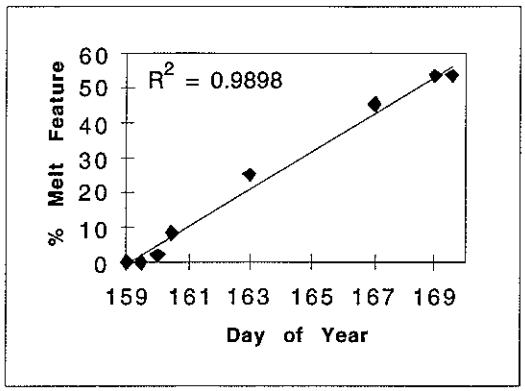

Figure 7. Percent area in the melt feature class.

As a means of exploring the spatial consistency of results, the study area images from Day 163, 165, and 169 were compared to supplementary images of first-year sea ice collected over different first-year sea ice areas on the same days. While the results indicate a close relationship in values (Table 2), additional supplementary first-year sea ice images would be necessary to more rigorously examine the reproducibility of these results.

Table 2. Comparison of intensive site and supplementary image results (snow cover:melt feature)

Day	*Intensive Ratio*	*Supplementary Ratio*	*Difference*
163	25:75	29:71	4%
167	55:45	54:46	1%
169	46:54	48:52	2%

CONCLUSIONS

A strong linear trend in the proportion of first-year sea ice covered by melt features has been calculated using a 10 day time series of imagery. In this relatively short period a sea ice surface with no melt features and a spatially consistent late winter albedo was transformed to over 50% standing water and a spatially erratic albedo influenced strongly by the different absorptive properties of water and snow. This rapid surface change is significant with respect to energy absorption and reflection at the ice/snow/water surface and for the acquisition of sea ice information by remote sensing during the melt season. This information can also be used to investigate the treatment of melt features in sea ice models, and can be linked to physical processes occuring at or near the ice surface.

DISCUSSION

1. Relevance to Sea Ice Modeling

Knowledge of the temporal rate of melt pond coverage and associated surface albedo is important as thermodynamic sea ice modeling efforts have shown sensitivity to parameters associated with melt feature area, depth, and surface albedo. Not only has it been observed that changes in surface albedo parameterization greatly influence model results (Shine and Henderson-Sellers, 1985), but there is also a degree of uncertainty regarding melting ice albedo values themselves. Maykut and Untersteiner (1971) used a melting ice albedo of 0.64 while other observations have led to estimates of 0.5 (Scharfen et al., 1987). Langleben (1968) has shown a 10 day change in albedo from 0.6 to 0.4 during spring melt which illustrates a rapid temporal rate of change. With this uncertainty regarding regional albedo values, knowledge of the local scale spatial fluctuations in melt feature coverage and corresponding albedo as discussed in this work can be very helpful. The reproducibility of the study results (Table 2) show that larger scale estimations of surface conditions can be attempted using the values derived from this study area.

Shine and Henderson-Sellers (1985) concluded that the representation of melting snow as a distinct albedo class is significant. This study has shown that transitional melt features like wet snow can be difficult to isolate as an image class because of overlapping pixel values with residual snow features. However, emphasizing image enhancement techniques significantly assists efforts to isolate this important type of surface class.

2. Surface Processes

The collection of micrometeorological data is an important component of the SIMMS field program, and this data set can be used to examine surface processes occurring during the evolution of melt features. Meteorological stations were established at first-year and multiyear sea ice sites and operated for the duration of the SIMMS field season. Monitored variables at the first-year site are shown in Table 3. Instrumentation was supported on a 5 meter main tower, 2 meter mini tower and a variety of wooden support structures. For a complete technical overview of the sites and instrumentation, see Derksen (1995).

Radiation Variables

Incident solar radiation ($K\downarrow$) was measured with an Eppley Black and White (B&W) pyranometer mounted on support beams independant of the main tower, while reflected shortwave radiation ($K\uparrow$) WAS measured with an inverted B&W pyranometer which was extended from the main tower. Incident solar radiation is very erratic during the spring season because of the frequent discontinuous periods of fog and low cloud during the spring season (Figure 8a). It is therefore difficult to establish a relationship between $K\downarrow$ and melt feature growth. As expected, daily average reflected solar radiation decreases in a near linear fashion as melt pond area increases (Figure 8b). The decrease in $K\uparrow$ is evident long before standing water appears, highlighting the necessity of classifying wet snow as a surface class with unique absorption quantities. Net all-wave radiation (Q^*) was monitored with a Middleton CN-1 pyrradiometer, also extended from the main tower. A similar linear trend to the rate of melt pond growth is noted (Figure 8c).

Temperature Variables

Profile air temperature data were collected at both sites in radiation shaded and ventilated shields using 24 AWG copper-constantan thermocouple sensors. Average daily air temperature from all first-year probes is shown in Figure 9a. No clear relationship between air temperature and ponding is evident. During the initial period of pond formation (Day 160 to 163) air temperatures decreases while the later stages of pond growth are matched with warming temperatures. Instead, pond growth appears to be closely associated with snow and ice temperatures.

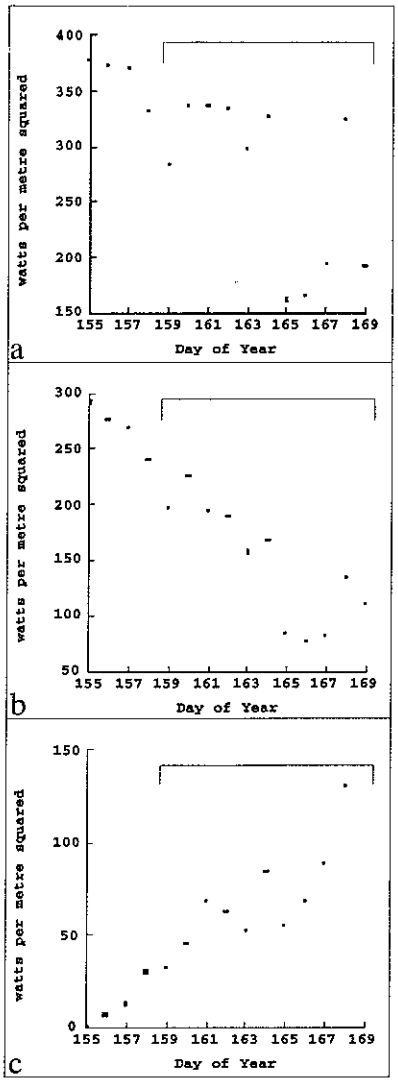

Figure 8. Daily average incident shortwave radiation (a) reflected shortwave radiation (b) and net all-wave radiation (c). Period of balloon flights is bracketed.

Snow temperature was measured in increments of 5 centimeters extending from the snow/ice interface to the snow surface. Each sensor consisted of a 24 AWG copper-constantan thermocouple junction imbedded at the tip of a brass tube. The tubes were epoxied in profile to a wooden stake and the whole array was painted white. Ice temperature arrays were similar in design, with thermocouple junctions imbedded into holes drilled into wooden dowel.

Average first-year snow pack temperature rises steadily from the late winter (Figure 9b) with the values levelling off at a maximum of approximately 1° C. The threshold snow temperature value for the presence of standing water was 0° C. The plot of daily average ice temperature (Figure 9c) is very similar to snow temperature with a maximum temperature of - 0.5° C at the end of the study period. Standing water appeared at an ice temperature of - 2.5° C.

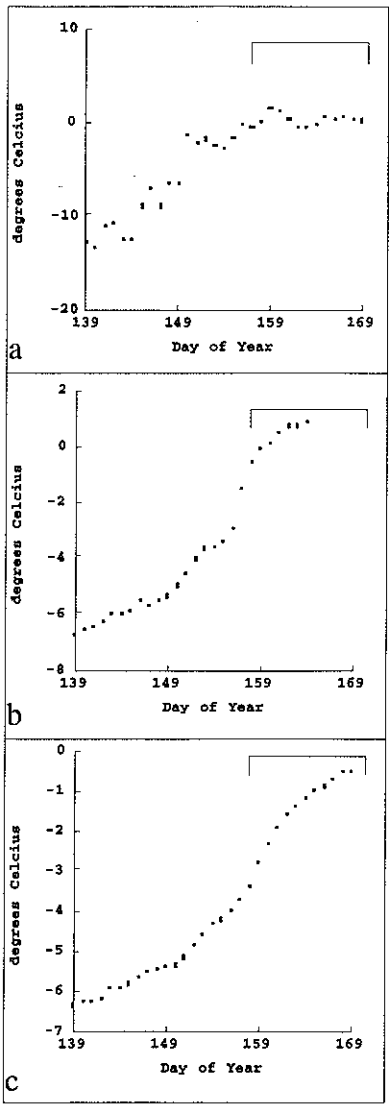

Figure 9. Daily average air temperature (a), snow pack temperature (b), and ice temperature (c). Period of balloon flights is bracketed.

This cursory overview is useful for examining how surface parameters change in accordance with the evolution of melt features. A complete set of micrometeorological field data is a valuable asset for continuing efforts to study melt feature growth and triggers to that growth.

3. Technical Considerations

It is important to consider technical issues in regards to the data collection and any impact they may have on results. Panchromatic and infrared images were collected simultaneously in the field, with infrared imagery used in this work. Preliminary

image comparison showed that the infrared data provides better contrast between melt features and snow cover than does panchromatic imagery. An in-depth comparison, however, could find applications more suited to the panchromatic data. It is also necessary to examine the influence lighting conditions at the time of photography have on image collection. As discussed earlier, diffuse versus unobscured lighting conditions made it impossible to select a consistent gray level threshold value. Cloud shadows also made image thresholding more difficult.

Nominal balloon flying heights were 300 and 100 meters, with a time series of imagery collected at both altitudes. While this study used the 300 meter data set for an increased study area, the improved resolution of the 100 meter imagery makes that another useful time series.

The variable nature of Arctic sea ice is clearly represented through the rapid evolution and growth of melt features. The dramatic changes in surface parameters such as albedo that are caused by the growth and spatial discontinuity of melt features makes the examination of that growth rate an important procedure. Low level aerial photographs, with a fine spatial and temporal resolution are ideal for monitoring melt pond formation and evolution. By emphasizing accurate post-field processing, utilizing a corresponding micrometeorological dataset, and potentially including surface measurements, these images constitute a valuable data source for exploring melt processes over sea ice.

ACKNOWLEDGMENTS

This work was supported by funding through the Natural Science and Engineering Research Council (Operating Grant - E. LeDrew) and the Northern Studies Scientific Training Program (Grants - C. Derksen and J. Piwowar). Special thanks are given to the Polar Continental Shelf Project for logistical support, and appreciation is extended to the SIMMS'95 field crew.

REFERENCES

Derksen, C. 1995. Section 3.1 Microclimatology in Misurak, K., C Derksen, D. Barber and E. LeDrew (eds.) SIMMS'95 Data Report. Earth Observations Laboratory Technical Report. ISTS-EOL-TR-95-003.

Derksen, C., J. Piwowar, and E. LeDrew. 1996. The quantification of sea ice melt features from low level aerial photographs. Proceedings, IGARSS'96 1:127 - 129.

Ebert, E., and J. Curry. 1993. An intermediate one-dimensional thermodynmaics sea ice model for investigating ice-atmosphere interactions. Journal of Geophysical Research. 98 (C6): 10 085 - 10 109.

Ingram, W., C. Wilson, J. Mitchell. 1989. Modeling climate change: An assessment of sea ice and surface albedo feedbacks. Journal of Geophysical Research. 94: 8609 - 8622.

Langleben, M. 1968. Albedo measurements of an Arctic ice cover from high towers. Journal of Glaciology. 7: 289 - 297.

Langleben, M. 1971. Albedo of melting sea ice in the Southern Beaufort Sea. Journal of Glaciology. 10: 101 - 104.

Maykut, G., and N. Untersteiner. 1971. Some results of a time dependant thermodynamic model of sea ice. Journal of Geophysical Research. 76: 1550 - 1575.

Piwowar, J. 1995. Section 2.4 Balloon Data in Misurak, K., C Derksen, D. Barber and E. LeDrew (eds.) SIMMS'95 Data Report. Earth Observations Laboratory Technical Report. ISTS-EOL-TR-95-003.

Russ, J. 1995. The Image Processing Handbook, 2nd Ed.

Scharfen, G., R. Barry, D. Robinson, G. Kukla, and M. Serreze. 1987. Large scale patterns of snow melt mapped from meteorological satellite imagery. Annals of Glaciology. 9: 200-206.

Shine, K., and A. Henderson-Sellers. 1985. The sensitivity of a thermodynamic ice model to changes in surface albedo parameterization. Journal of Geophysical Research. 90: 2243 - 2250.